Vol. 24 • No. 44 • November 26 • 2014

www.afm-journal.de

ADVANCED FUNCTIONAL MATERIALS

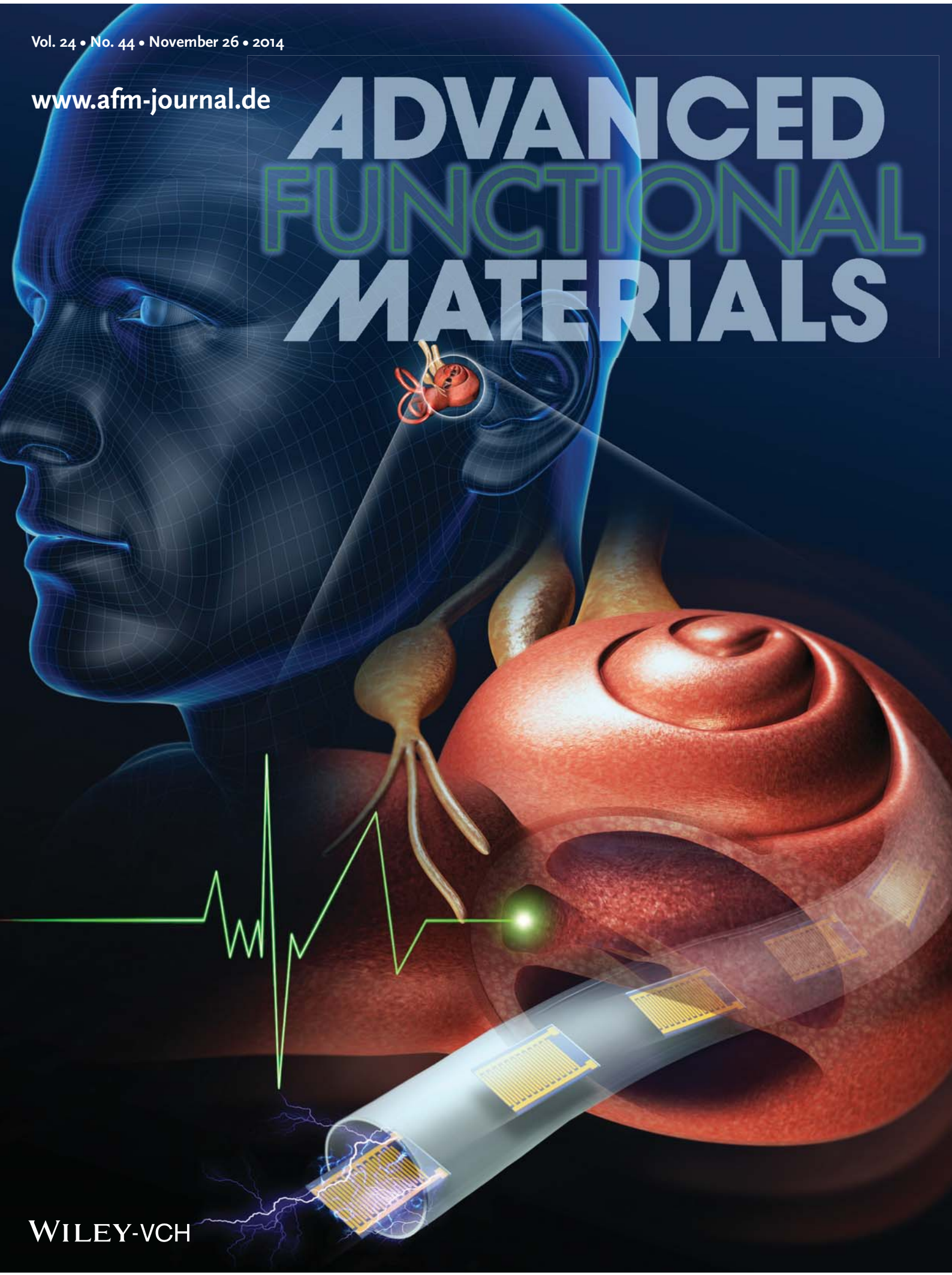

WILEY-VCH

ADVANCED FUNCTIONAL MATERIALS
www.afm-journal.de

Materials Views
www.MaterialsViews.com

Flexible Inorganic Piezoelectric Acoustic Nanosensors for Biomimetic Artificial Hair Cells

Hyun Soo Lee, Juyong Chung, Geon-Tae Hwang, Chang Kyu Jeong, Youngdo Jung, Jun-Hyuk Kwak, Hanmi Kang, Myunghwan Byun, Wan Doo Kim, Shin Hur, Seung-Ha Oh,* and Keon Jae Lee**

For patients who suffer from sensorineural hearing loss by damaged or loss of hair cells in the cochlea, biomimetic artificial cochleas to remedy the disadvantages of existing implant systems have been intensively studied. Here, a new concept of an inorganic-based piezoelectric acoustic nanosensor (iPANS) for the purpose of a biomimetic artificial hair cell to mimic the functions of the original human hair cells is introduced. A trapezoidal silicone-based membrane (SM) mimics the function of the natural basilar membrane for frequency selectivity, and a flexible iPANS is fabricated on the SM utilizing a laser lift-off technology to overcome the brittle characteristics of inorganic piezoelectric materials. The vibration amplitude vs piezoelectric sensing signals are theoretically examined based on the experimental conditions by finite element analysis. The SM is successful at separating the audible frequency range of incoming sound, vibrating distinctively according to varying locations of different sound frequencies, thus allowing iPANS to convert tiny vibration displacement of ≈15 nm into an electrical sensing output of ≈55 μV, which is close to the simulation results presented. This conceptual iPANS of flexible inorganic piezoelectric materials sheds light on the new fields of nature-inspired biomimetic systems using inherently high piezoelectric charge constants.

1. Introduction

About 10% of the population globally experiences moderate to severe congenital or acquired hearing impairment,[1] with such impairment thus presenting a higher frequency of occurrence than diseases such as cancer, cardiopathy, and tuberculosis. The major causes of hearing impediments are extremely diverse and include age, noise, illness, medications, and chemical or physical trauma. Sensorineural hearing loss (SNHL) is a representative hearing impairment caused by dysfunction of frequency discrimination and is mainly triggered by the loss of hair cells of the organ of *Corti* in the cochlea.[2,3] Hair cells, which locate all along the basilar membrane (BM), convert sound-induced vibration of BM into electricity to stimulate auditory nerves. Most cases of SNHL are irreversible since these hair cells are not able to regenerate.[4–6]

Cochlea implants, which convert acoustic energy from external sound into electricity to stimulate auditory nerves through an electrode array inserted in the cochlea, are a widely used technology for treating profound SNHL.[7,8] However, such systems have disadvantages of discomfort caused by the use of extracorporeal devices, large power, and low speech recognition due to a small number of electrodes. To overcome these weaknesses, developing an artificial cochlea without an exterior power supply has been the focus of efforts by many researchers worldwide.[9–15] Recently, Inaoka et al. demonstrated an artificial cochlea epithelium using an

H. S. Lee, G.-T. Hwang, C. K. Jeong, Dr. M. Byun, Prof. K. J. Lee
Department of Materials Science and Engineering
Korea Advanced Institute of Science and Technology (KAIST)
291 Daehak-ro, Yuseong-gu, Daejeon 305–701, Republic of Korea
E-mail: keonlee@kaist.ac.kr

H. S. Lee
Electronic Materials Research Institute
Kolon Central Research Park, 154 Mabuk-ro, Giheung-gu
Yongin, Gyeonggi-do 446–797, Republic of Korea
E-mail: shaoh@snu.ac.kr

Dr. J. Chung, Prof. S.-H. Oh
Department of Otorhinolaryngology
Seoul, National University College of Medicine
101 Daehak-ro, Jongno-gu, Seoul
110–744, Republic of Korea

Dr. J. Chung
Department of Otolaryngology
Ajou University School of Medicine
164 World Cup-ro, Yeongtong-gu,
Suwon, Gyeonggi-do 443–380 Republic of Korea

Dr. Y. Jung, J.-H. Kwak, H. Kang,
Dr. W. D. Kim, Dr. S. Hur
Department of Nature-Inspired Nanoconvergence System
Korea Institute of Machinery and Materials
156 Gajeongbuk-ro, Yuseong-gu, Daejeon 304–343, Republic of Korea
E-mail: shur@kimm.re.kr

DOI: 10.1002/adfm.201402270

organic piezoelectric membrane to mimic the functions of mammalian hair cells.[15] A polyvinylidene fluoride (PVDF) membrane was placed at the BM of the cochlear to detect the natural motion of the BM in response to sound stimuli and converted its motion into electrical output to operate auditory nerves. However, the electrical output power was not sufficient to stimulate the auditory nerves directly because the piezoelectric charge constant of an organic piezomaterial, a crucial parameter for determining electrical output, is relatively low. One solution to enhance electric output performance is by utilizing inorganic piezoelectric materials, which have an inherently high piezoelectric charge constant (d_{33}).[16] However, with the use of inorganic materials, it is difficult to secure flexibility owing to their brittle properties. To date, several researchers have centered on research to realize flexible inorganic piezoelectric materials for demonstration of high performance flexible energy harvesting systems,[17–24] but relatively little effort has been devoted to sensors for biomedical applications. Recently, our group successfully demonstrated an exceptionally efficient flexible piezoelectric energy harvester enabled by crystallized $Pb[Zr_xTi_{1-x}]O_3$ (PZT)[23] or a single-crystal PMN-PT[24] thin film transferred onto a flexible plastic substrate.

Here, we report a highly efficient and flexible inorganic piezoelectric acoustic nanosensor (iPANS) using a PZT thin film for the purpose of biomimetic artificial hair cells. A laser lift-off (LLO) process is utilized for transferring a PZT thin film from a bulk wafer to a flexible plastic substrate without any mechanical defects to realize a flexible iPANS. The capability of the frequency selectivity of a trapezoidal silicone-based membrane (SM), which corresponds to the function of the natural BM, is successfully confirmed based on the observation that the vibration of the SM occurred at different local places according to the frequency of incoming sound waves. Vibration displacement of the SM and the piezoelectric signal generated by iPANS are measured using a laser Doppler vibrometer (LDV) and a sound level analyzer, respectively, and vibration displacements of 7 nm to 17 nm and piezoelectric signals of 45 μV to 60 μV are obtained. The theoretical calculation of 51.7 μV simulated by the finite element analysis (FEA) method strongly supports the experimental sensing output during vertical deformation of SM. In addition, the distribution of vibration displacements measured by LDV overlaps remarkably well with the distribution of the corresponding piezoelectric output signals in a frequency range of 100 Hz to 1600 Hz. Consequently, the iPANS achieves highly efficient sensitivity and electrical output from a tiny motion (≈15 nm) of SM in response to acoustic stimuli in the range of audible frequency.

2. Results and Discussion

Figure 1a shows conceptual schematic drawings describing the organ of Corti and the flexible PZT film beneath the BM with response to sound stimuli. As schematically drawn in Figure 1a, both the inner and outer hair cells are positioned normal to the BM. These hair cells play critical roles in transmitting, amplifying, and filtering sound vibration. For sound propagation, the initial sound wave can be transmitted to the brain by the inner hair cells, whereas the sound frequency can be fine-tuned by the outer hair cells with somatic electromotility.[25–28] The shear motion of the hair cells is driven by the oscillatory motion of the BM. The oscillatory motion of the BM near the base of cochlea can be amplified by high-frequency sounds, whereas its motion near the apex of the cochlea can be amplified by relatively low-frequency sounds due to variation of the BM width, thickness, and stiffness along the length of the cochlea spiral.[14,29,30] These vibrational motions of the BM lead the hair cells to generate electricity, thus stimulating the auditory nerves. If these hair cells are lost or damaged by various factors, the damaged hair cells no longer generate an electrical potential, resulting in permanent hearing impairment such as SNHL. To treat this dysfunction, artificial hair cells using piezoelectric materials are expected to be a strong substitute for impaired hair cells. They would function by attaching to the natural BM, which is still alive in most cases of deafness regardless of damaged hair cells. In this study, a theoretical approach was taken to identify the electrical response of a flexible PZT film to the motion of the BM by a FEA simulation method using COMSOL software (bottom right of Figure 1a). Since the vertical displacement of the natural mammalian BM in response to sound is approximately 600 nm,[15] the simulated PZT film was bent at a height of 600 nm. As a result, the simulated piezopotential from the PZT film was approximately 3 V, which is sufficient power to simulate the auditory nerves without an additional power supply (see the Experimental Section for more details of the simulation method). Based on this simulation, a flexible iPANS was designed onto the artificial silicone-based BM to mimic the function of natural hair cells.

Figure 1b shows the fabrication process of the flexible iPANS. i) A 2μm thick PZT film (1.0 cm × 1.0 cm) on a bulk sapphire wafer was thermally treated by a rapid thermal annealing system at 650° for 45 min for the crystallization of high performance piezoelectric thin film. ii) A flexible supporting substrate (PET substrate) was bonded to the PZT film by an ultraviolet (UV) curable polyurethane (PU) adhesive with UV light. iii) The bulk sapphire wafer was removed from the PZT film via the LLO process. iv) Interdigitated electrodes (IDEs) were patterned on the PZT film with Au deposition by radio frequency (RF) sputtering (see Supporting Information Figure S1 for more details regarding the fabrication of the flexible iPANS). v) Finally, a single flexible iPANS was firmly fixed onto the surface of a SM frequency separator with double sided adhesive tape. The frequency separator consists of a freestanding trapezoidal SM covering an acrylic plate with a trapezoidal slit, as shown at the bottom of Figure 1b; the trapezoidal SM over the slit corresponds to the natural BM, which spatially separates the frequencies of incoming sound.[11,31] Figure 1c shows a schematic diagram of a vibrating SM in response to an incoming acoustic wave. The iPANS units were distantly placed at the SM to precisely detect the motion of the vibrating SM. When the acoustic wave is incident on the frequency separator, the freestanding SM vibrates due to a resonance effect, and hence the iPANS on top of the SM is mechanically deformed by the sound-driven vibration of the SM, as shown in the inset of Figure 1c. Deformation of the iPANS leads to a change of the dipole state inside the flexible PZT film of iPANS, and thus it converts the sound-driven vibration to electricity by the piezopotential difference of the internal PZT film. Figure 1d shows

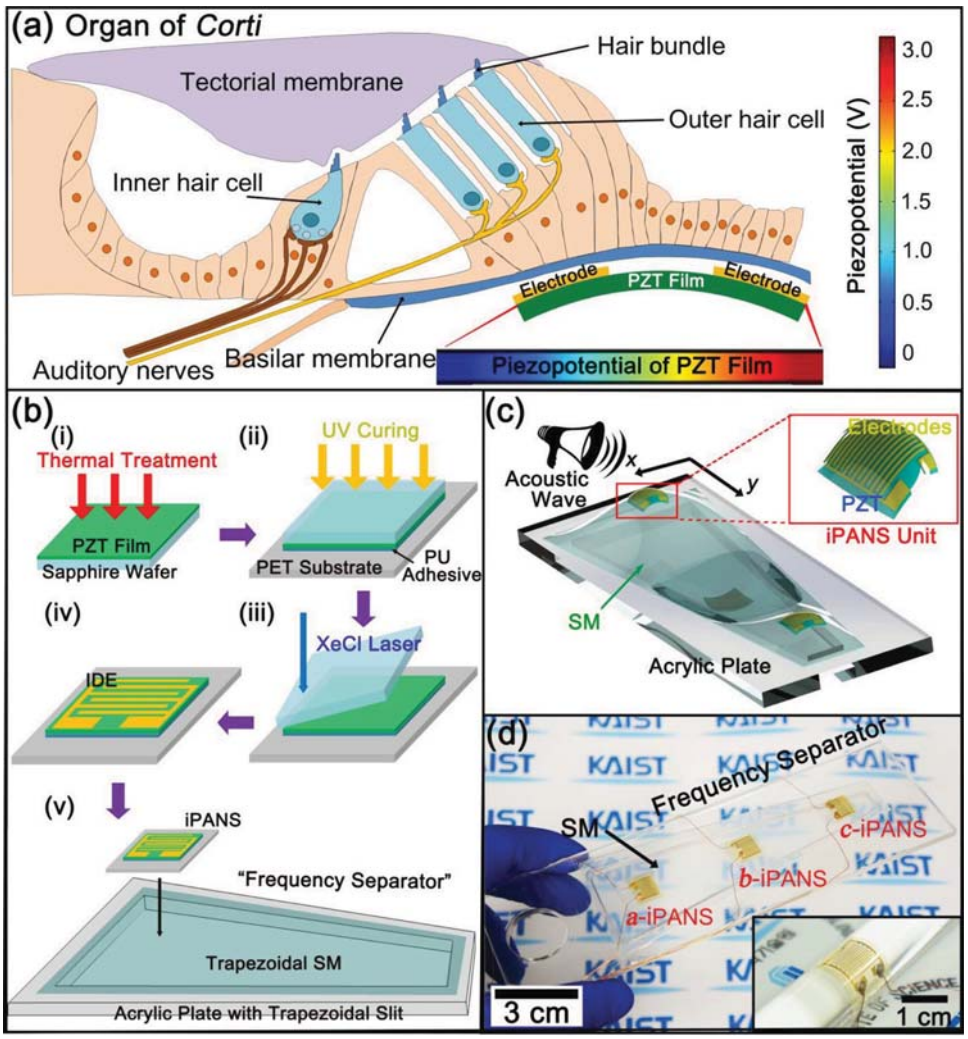

Figure 1. a) Conceptual schematics of organ of *Corti* in mammalian cochlea. Thin PZT film was placed under BM, and vibrates in the same manner as BM according to sound wave. When a tensile stress applied parallel to the surface of PZT film, the PZT film was bent upwards with a height of 600 nm and generated piezopotential of ≈3 V. b) Fabrication steps for iPANS i) Coat PZT film on a sapphire wafer is thermally treated for its crystallization via RTA process. ii) PZT film bonded onto a flexible supporting substrate (PET substrate) with PU adhesive and is cured by UV light. iii) The sapphire wafer is removed from the PZT film with XeCl laser beam via LLO process. iv) Au IDE patterned on the flexible PZT film. v) The flexible iPANS attached onto the frequency separator, which is made up of a trapezoidal SM covering acrylic plate with trapezoidal slit. c) According to acoustic wave, SM vibrated due to resonance; iPANS is mechanically deformed in response to vibration, resulting in converting into electricity. d) Photograph of the frequency separator with iPANS. The inset shows a single iPANS unit attached to a glass rod with a radius of curvature of 1.0 cm.

a photograph of the SM frequency separator with *a*-iPANS, *b*-iPANS, and *c*-iPANS arranged at the apex, intermediate, and base area of the SM, respectively. The inset of Figure 1d shows a flexible single iPANS adhered to a glass rod with a radius of curvature of 1.0 cm, confirming high flexibility and mechanical stability of the iPANS.

Device performance of the flexible iPANS strongly depends on characteristic microstructures of the PZT piezomaterials realized by our optimized LLO transfer process. To confirm that there are no substantial changes of high quality crystallographic features before and after the LLO process, we conducted compositional and structural analyses of the PZT films on both a bulk sapphire wafer and a flexible substrate using X-ray diffraction (XRD) and Raman spectroscopy, respectively. **Figure 2**a,b shows the XRD analysis results of the PZT film on the bulk sapphire wafer before the LLO process and the flexible substrate for iPANS after the LLO process. To distinguish the rhombohedral and tetragonal crystalline phases in the PZT samples, the XRD (111) and (002) peaks were clearly compared, confirming that there is not a substantial phase change after the LLO process, as shown in Figure 2b. For both conditions, perovskite (100) and (200) peaks remained consistently. The insets of Figure 2a,b show cross-sectional scanning electron microscopy (SEM) images of the crystallized PZT film on the sapphire wafer (i.e., before LLO process) and the flexible substrate (i.e., after LLO process), respectively. Mechanical damage or thermally driven defects of the piezoelectric film caused by laser irradiation were not observed on either side of the PZT film. Figure 2c,d show the Raman spectra of the PZT film before and after the LLO process at room temperature. The spectra are very similar for both

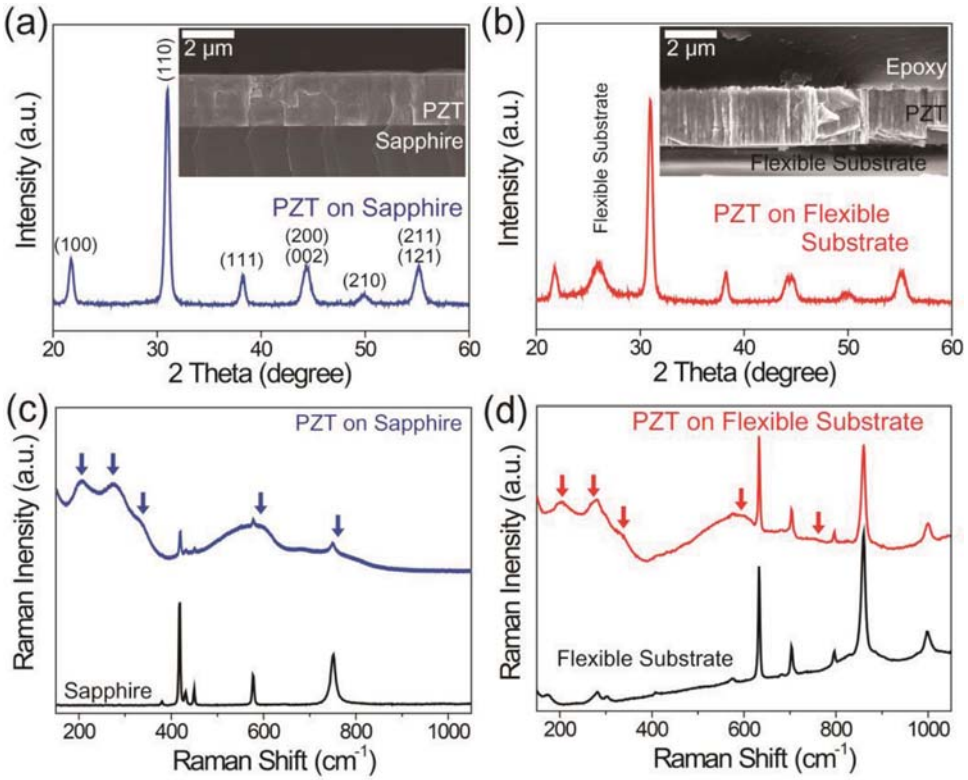

Figure 2. a) XRD analysis result of PZT film on a bulk sapphire wafer before transfer process. The inset shows SEM image of PZT film on the sapphire wafer. b) XRD analysis result of PZT film on a flexible substrate after transfer process. This inset shows SEM image of PZT film on the flexible substrate and covered by SU8 epoxy. c) Raman spectra of PZT film on the sapphire wafer before transfer process. The curves indicated by arrows show the archetypal perovskite PZT phase. d) Raman spectra of PZT film on the flexible substrate after transfer process.

conditions, indicating that the perovskite PZT phase was maintained despite the surface discrepancy inevitably induced by laser overlapping. An archetypal perovskite PZT phase is well-expressed by the curves indicated by the arrows in Figure 2c.[32,33] Likewise, the curves of the iPANS PZT film on the flexible substrate correspond to the position of a high quality perovskite PZT Raman shift, as shown in Figure 2d. This result confirms that the rigid PZT film on the bulk wafer was safely transferred to the flexible substrate for iPANS through the optimized LLO process.

Figure 3a presents the working mechanism for generating electricity under sound-driven pressure applied to the flexible iPANS. The sound-driven vibration of the SM in response to incoming sound causes bending deformation of the flexible iPANS on the SM. The polarized dipoles are likely to be aligned parallel to the surface of the PZT film between adjacent electrodes (Figure 3a,i). According to piezoelectricity theory, once a polycrystalline piezoelectric ceramic, such as a PZT material, is subjected to a poling process under a strong electric field at high temperature, most of the dipole, which is randomly aligned owing to the isotropic polarization domains, is uniformly aligned parallel to the direction of the applied electric field, and its polarity remains permanently even after the electric field is removed.[34] When the flexible iPANS PZT film is bent by sound-driven pressure, as shown in Figure 3a,ii, it causes the ions within the polarized dipoles to change their condition, change of dipole moment, and consequently a piezoelectric potential difference between adjacent electrodes can be generated instantaneously, and at the same time, electrons flow in the external circuit. The piezoelectric potential (E) can be defined by applied sound-driven mechanical stress and the

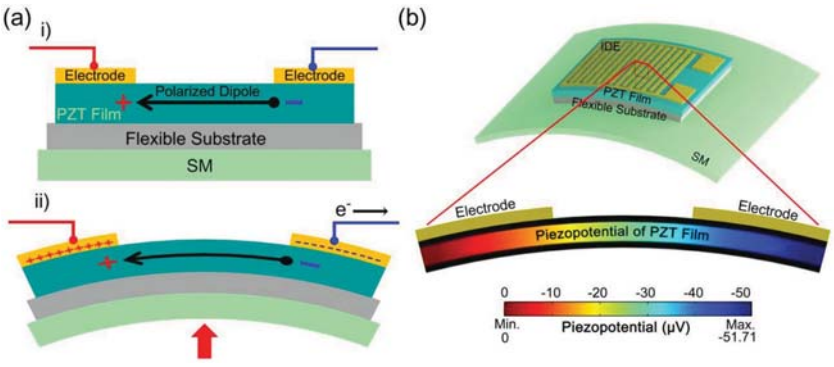

Figure 3. a) Schematics of the working principle in generating piezoelectricity of iPANS unit i) before and ii) after bending deformation. b) Simulated piezopotential distribution inside a PZT film between adjacent electrodes. The dimension of simulated model corresponds to that of actual model.

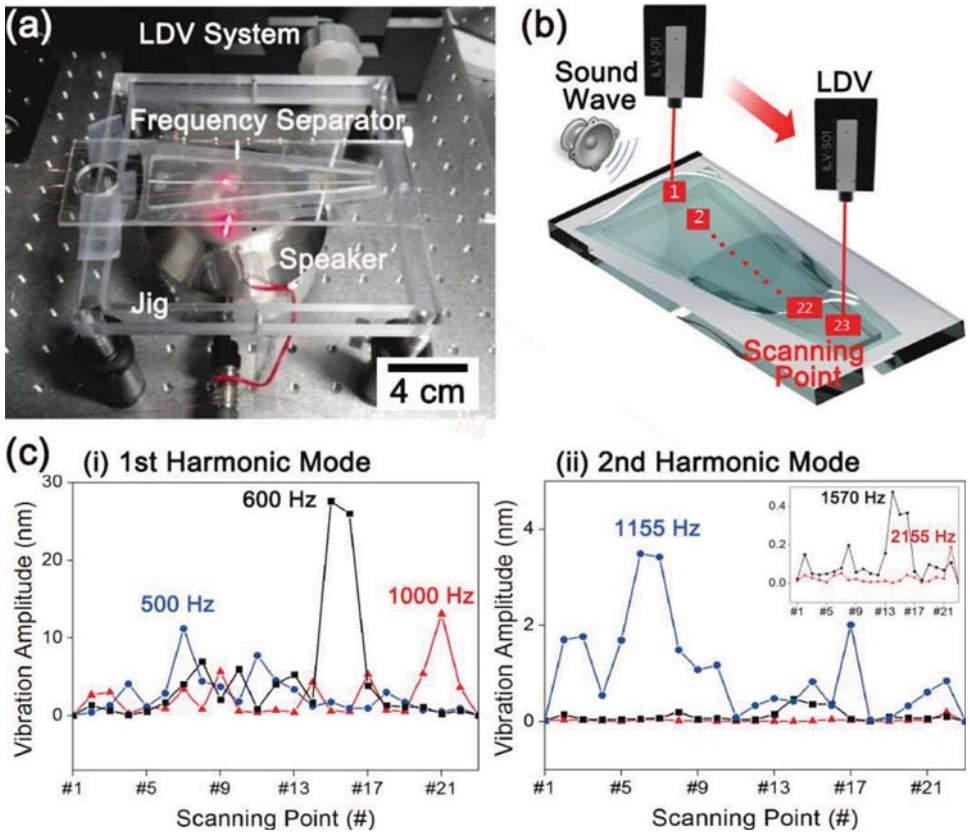

Figure 4. a) Experiment setup with several apparatuses for measuring the vibration amplitude of iPANS in response to the sound coming from a speaker. b) LDV system scanned point by point over all longitudinal-axis of SM. Total 23 scanning points were observed. c) Peak of vibration over all scanning points in i) 1st harmonic mode and ii) 2nd harmonic mode. Most of vibration amplitude in 2nd harmonic mode was under 5 nm, which is much smaller than that of 1st harmonic mode.

piezoelectric charge constant ($d_{ij} = g_{ij}\varepsilon^T$, where g_{ij} and ε^T are the piezoelectric voltage constant and the permittivity at constant stress, respectively), and can be expressed as follows:

$$E = \frac{D - d_{ij}T}{\varepsilon^T} \quad (1)$$

where T and D indicate the applied sound-driven stress to the flexible iPANS and the piezoelectric potential of dipole inside iPANS PZT piezo-materials, respectively. When the stress is applied to the piezoelectric materials, the electric field (E_1) is expressed as $(D–d_{ij}T)/\varepsilon^T$, whereas when stress is not applied to the piezoelectric materials, the electric field (E_2) is simplified as D/ε^T. The sound-driven piezoelectric potential difference (ΔE) is finally defined by $-(d_{ij}T)/\varepsilon^T$. The piezoelectric potential strongly depends on both the piezoelectric charge constant and the applied sound-driven stress.[35] This theoretical interpretation indicates that inorganic piezoelectric materials, which have an inherently high piezoelectric charge constant, should show high performance in generating piezoelectricity.

Figure 3b shows the piezopotential of the flexible PZT film used for the iPANS upon bending deformation estimated by the FEA method using COMSOL software to further support the working mechanism of the flexible iPANS. The simulated model was bent upwards with a height of 15 nm, which is much lower than that of the mammalian BM (≈600 nm), because the SM vibrates at ten orders less than the natural BM due to its bulky, heavy, and elastic properties.[9] The theoretically calculated piezopotential distribution inside the color-coded PZT film was approximately –51.71 μV between adjacent electrodes. This simulation result supports that the piezoelectric material is capable of converting sound energy at even nm-level into electrical energy.

We now analyze the tuning capability of the frequency separator with frequency selectivity. Before attaching the iPANS to the SM, we first investigated vibration amplitudes with response to arbitrarily applied sound waves using a LDV system. The laser Doppler vibrometer (LDV) system emits a laser beam into a vibrating object and measures the vibration velocity of the object by the difference in frequency of the incident beam and the reflected beam having Doppler effects.[36] **Figure 4**a shows the experimental setup for analyzing the vibratory property of the frequency separator. A frequency separator fixed on a jig was placed onto a stationary table to diminish any potential effects of ambient vibrations. A speaker, which was equipped under the frequency separator, produced white noise sound (frequency bandwidth from 3.125 Hz to 20 kHz and approximately 40 dB SPL of sound pressure) towards the frequency separator and caused the SM frequency separator to vibrate due to resonance. The amplitude and occurrence location of

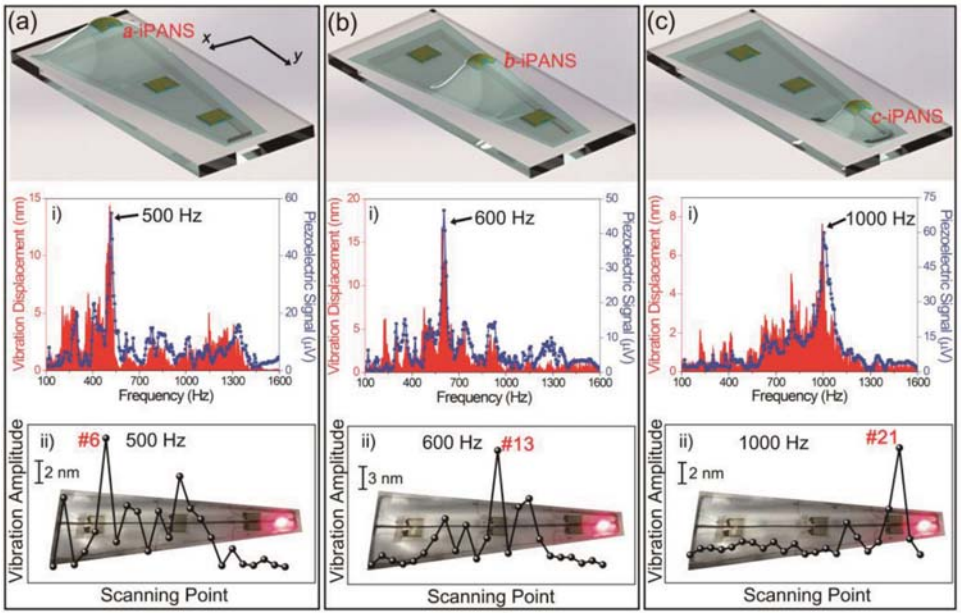

Figure 5. A vibration displacement and a piezoelectric signal generated by a,i) a-iPANS, b,i) b-iPANS and c,i) c-iPANS measured by LDV system and a sound level analyzer, respectively, in the frequency range of 100 Hz to 1600 Hz. A distribution of the vibration displacement and the piezoelectric signal were closely overlapped all over the frequency bandwidth. A single peak of vibration amplitude in response to a,ii) 500 Hz, b,ii) 600 Hz, c,ii) 1000 Hz appeared at 6th, 13th, 21st, respectively.

the vibration depended on the frequency of incoming sound,[31] which was measured using the LDV system. Figure 4b schematically illustrates the scanning process of the LDV system, which was equipped perpendicular to the frequency separator to longitudinally scan over 23 sections (1st and 23rd scanning points corresponding to the apex and the base regions) of the SM, collecting the vibration amplitude at each section. Figure 4c,i shows the peak of vibration throughout all the scanning points to investigate the vibratory behavior of the SM frequency separator without iPANS units at the first harmonic mode. The local region, where the local resonance frequency of the SM matches that of the incoming sound, vibrates with relatively large amplitude, resulting in a peak of vibration. The 7th scanning point corresponded to the local region of the SM with a peak of vibration at 500 Hz. Similarly, the local regions with vibration amplitudes at 600 Hz and 1000 Hz corresponded to the 15th and 21st scanning points, respectively. Predominantly, the peak of vibration tended to be shifted towards higher scanning points, corresponding to the base region of the actual BM, as the sound frequency increased. This phenomenon was consistent with the second harmonic mode,[37] as clearly shown in Figure 4c,ii. The peak of vibration that occurred at the 6th scanning point corresponding to 1155 Hz started to shift towards the 22nd scanning point (inset of Figure 4c,ii) as the frequency was increased from 1155 Hz to 2155 Hz. Briefly, as a harmonic mode is periodically repeated, the vibration amplitude is likely to be weakened. This experimental observation shows the identical capability for frequency selectivity as the mammalian BM, where each local region resonates at two or more frequencies.[38] In short, the frequency separator was successful in separating the incoming sound frequency, similar to the actual BM. On the basis of this experimental observation, individual iPANS units were arranged in three local areas at which the maximum vibration amplitude can convert an oscillatory motion into a piezoelectric signal. This setup was motivated by confirming the frequency selectivity of the frequency separator in response to varied sound frequencies.

We finally investigated a sound-driven piezoelectric signal and a vibration displacement generated by iPANS, and the peak of vibration at each resonance frequency, as described in **Figure 5**. According to three representative frequency points (500, 600, and 1000 Hz, as seen in Figure 4c), three iPANS units were arranged along the y-direction of the SM (*a*-, *b*-, and *c*-iPANS units positioned at the 6th, 13th, and 21st scanning points, respectively), as schematically illustrated in Figure 5a–c. Upon an incoming sound wave with a frequency range of 100 Hz ≈ 1600 Hz, each iPANS unit at three positions resulted in a comparable distribution between the piezoelectric signal and vibration displacement, as shown in Figures 5a,i, 5b,i, and 5c,i. The sound pressure provided by the speaker was approximately 40 dB SPL, which is equivalent to living noise and much lower than a home voice. Regarding the SM reaction to very slight noise, the resulting vibration displacements closely matched the piezoelectric signals within the frequency bandwidth. This comparison indicates that the iPANS used in this study was greatly sensitive to the entire oscillatory motions of the SM within the audible frequency range. In addition, the iPANS converted sound-driven vibration of the SM into piezoelectric signals, corresponding with the function of natural hair cells. At three representative frequency points (500 Hz, 600 Hz, and 1000 Hz), oscillatory displacements of the SM were measured as 14.4 nm, 16.8 nm, and 7.6 nm, which were directly related to conversion of mechanical fluctuations into piezoelectric signals of 54.8 μV, 46.6 μV, and 59.7 μV, respectively, by the iPANS. These piezoelectrical outputs were in good agreement with the theoretical calculation of 51.7 μV generated by the simulated

model in Figure 3b. The iPANS on the SM was normally implemented by the working principle of piezoelectiricity in generating electricity. It is worth noting that there was no frequency dependence of vibration amplitude and piezoelectric potential (i.e., an increase in the sound frequency did not lead to any direct decrease in vibration amplitude and the piezoelectric signal). Theoretically, the output piezoelectricity converted from a mechanical oscillatory motion should strongly rely on the sound frequency (i.e., the piezoelectric signal is decreased as the sound frequency increases). In the present study, because of a local stress relaxation effect induced by central drooping of the elastic silicon membrane along the x-direction, no clear frequency dependence of the piezoelectric potential was observed. This hanging phenomenon of the elastic SM is expected to be decreased as the lateral dimension along the x-direction is decreased.[9–11] Further study of the frequency effect on the output piezoelectricity should be carried out by changing the elasticity or thickness of the SM. In the present study, we placed emphasis on demonstrating the sensing capability of the iPANS.

Interestingly, there was no substantial change in the representative peak positions of the highest vibration amplitudes at three scanning points in response to varied sound frequencies (6^{th} scanning point: 500 Hz, 13^{th} scanning point: 600 Hz, 21^{st} scanning point: 1000 Hz) after attaching the iPANS units onto the SM. Slight dimensional changes of the SM in terms of thickness, stiffness, and weight due to attachment of the iPANS units showed no significant fall-off in the capability of frequency selectivity (Figure 5a,ii, b,ii, and c,ii).

In particular, numerical calculation of the piezoelectricity of the iPANS using a COMSOL simulation (in Figure 3b) was close to the experimentally measured piezoelectricity. These findings may open a potential route to the fabrication of implantable iPANS units with high electrical output to directly stimulate the auditory nerves and moreover to develop a fully implantable artificial hair cell, as illustrated in Figure 1a. The present study will be further extended to increase the number of iPANS units for filtering the sound frequency within a wider range as mammalians have tens of thousands of hair cells. In future study, the iPANS unit should be miniaturized to be suitable for insertion in the cochlea by utilizing the advanced semiconductor process technology, thus further improving the frequency discrimination.

3. Conclusions

In summary, we have proposed a new strategy to mimic the function of natural hair cells using a flexible inorganic piezoelectric acoustic sensor (iPANS), which may provide an effective means of treating hearing impairments (e.g., SNHL, deafness). A flexible iPANS was fabricated on SM, a highly sensitive membrane by sound-driven vibration, with a LLO transfer process. During the LLO transfer process, no significant changes in the microstructure or composition of the well-crystallized piezoelectric PZT film were observed. A frequency separator made of SM showed stable frequency selectivity to the incoming sound, mimicking the function of the natural BM. The sound-driven vibration of the SM sufficiently induces bending deformation of the iPANS. The iPANS showed excellent sensitivity, effectively converting sound energy into piezoelectric signals in the audible frequency range of living noise (40 dB SPL). Use of high performance iPANS units was beneficial for aligning the distribution of vibration displacement closely with that of the piezoelectric signals. To support the experimental results, a FEA simulation was conducted to rationalize the mechanism for piezoelectricity driven by iPANS as well as to secure the practical feasibility of an implantable iPANS into the cochlea. We are currently investigating a specialized process for inserting plural arrays of miniaturized iPANS, which can be a strong candidate for damaged hair cells, into a mammalian cochlea for treating SNHL.

4. Experimental Section

Fabrication Process for Flexible iPANS: To form a uniform PZT thin film on a bulk sapphire wafer (Hi-Solar Co., 430 μm in thickness), a 0.4 M PZT chemical solution (52/48 composition ratio of Zr/Ti with PbO 10 mol%, MEMS Solution Co.) was spin-coated on the wafer at 2500 rpm for 25 s and was thermally treated by rapid thermal annealing (RTA) at 450 °C for 10 min to remove organic components. A single cycle of these processes gave a PZT thin film with a thickness of 100 nm, and thus a total of 20 cycles were conducted to attain a thickness of 2 μm. Finally, the PZT film was thermally treated at 650 °C for 45 min for its crystallization. Subsequently, a flexible plastic substrate (50 μm, Kolon Industries Inc.) was bonded onto the top surface of the PZT film on the wafer by ultraviolet (UV) curable polyurethane (PU, Norland optical adhesive, No. 71); and then UV light was exposed for 30 min to strongly cure the PU layer between the PZT film and the PET substrate. Afterward, the sapphire wafer was removed from the resulted device with XeCl laser beam (wavelength of 308 nm). The used laser has energy of ≈420 mJ cm^{-2} and a pulse frequency of 10 Hz. The spot size for laser irradiation on the sample was 625 μm^2, and the laser scan speed was 3.7 mm s^{-1}. The overlapped width by consecutive laser irradiation was measured to be 55 μm. Cr/Au was deposited on the flexible PZT film via radio frequency (RF) sputtering for interdigitated electrode (IDEs, 100 nm thick Au) patterning. IDEs with an electrode width of 200 μm, an interelectrode gap of 200 μm, and 8 finger pairs were deposited on the PZT surface. SU8 epoxy was coated on the surface of the PZT film to prevent mechanical damage during the poling process and to acquire mechanical stability. Lastly, the device was subjected to an electric field of 1.0 kV cm^{-1} for 2 h for poling process.

Fabrication of the Frequency Separator: A trapezoidal SM (50 μm thick) was strainedly covered over an acrylic plate with a trapezoidal slit with adhesive glue. The width of the trapezoidal slit was linearly varied in a range of 10.0 mm to 35.0 mm in a gradient fashion along the longitudinal direction (i.e., length of 200 mm). The size of the trapezoidal SM was designed to be 10 mm larger than the slit. An optically reflective tape (15 μm thick) was attached at the center-axis of the SM to be measured by LDV system even after placing the iPANS unit on the SM surface.

Experimental Setup for Mechanical and Electrical Analyses of the Frequency Separator with iPANS: A speaker (4227, B&K, Nærum) was located under the frequency separator to produce an acoustic wave in a frequency range of 3.125 Hz ≈ 20 kHz with a step interval of 3.125 Hz. A LDV system (PSV-I-400 LR and OFV-505, Polytec) was equipped perpendicular to the frequency separator and horizontally scanned 23 sections along the longitudinal direction of the SM, thus measuring the vibratory behaviors of the SM at every section. For attaching the iPANS unit at more accurate position, the interval between scanning points was calculated using installed software in LDV system, and was marked on the surface of SM by pen. Subsequently, hte iPANS units were placed at the marked scanning point on the SM. Every measurement of the scanning process by the LDV was repeated

20 times to obtain a reliable average value to minimize experimental uncertainty. The piezoelectric output signals from the electrical pads were acquired with high accuracy data acquisition (DAQ) module (NI Pxle-4497, National Instruments). Output signals of the iPANS units were connected with the negative and positive probes of the sound level analyzer to transmit the piezoelectric signals when the SM vibrated in response to acoustic waves introduced by the speaker.

Simulation Method for an Artificial Hair Cell using a Flexible PZT Film: The simulated dimensions of the PZT film were 300 μm (width) × 300 μm (length) × 2 μm (thickness) and a pair of electrodes was located on the top surface of the iPANS. The electrode size was 100 μm (width) × 300 μm (length) × 100 nm (thickness) and the inter-electrode gap was 100 μm between adjacent electrodes. When tensile stress was applied parallel to the surface of the PZT film until a bending height of 600 nm, a piezopotential inside the PZT film was generated between neighboring electrodes.

Simulation for Working Mechanism of iPANS During Bending Deformation: The thickness and width of the electrode, PZT film, PET substrate, and SM are 100 nm/200 μm, 2 μm/1.0 cm, 50 μm/1.0 cm, and 50 μm/2.2 cm, respectively, which are dimensionally equivalent with the actual model. When a tensile stress of 1.2×10^{-8}% was applied to both sides of the SM in a parallel direction to the surface, the SM was mechanically bent upwards with a height of 15 nm, and thus led the iPANS to bend upwards with the same height.

Supporting Information

Supporting Information is available from the Wiley Online Library or from the author.

Acknowledgements

This work was supported by the Basic Science Research Program (grant code: NRF-2012R1A2A1A03010415) and Pioneer Research Center Program (NRF-2013M3C1A3042085) funded by the Korea government (MSIP) through the National Research Foundation of Korea (NRF).

Received: July 9, 2014
Revised: August 5, 2014
Published online: September 2, 2014

[1] N. Oishi, J. Schacht, *Expert Opin. Emerging Drugs* **2011**, *16*, 235.
[2] A. S. Nordmann, B. A. Bohne, G. W. Harding, *Hearing Res.* **2000**, *139*, 13.
[3] T. Endo, T. Nakagawa, T. Kita, F. Iguchi, T. S. Kim, T. Tamura, K. Iwai, Y. Tabata, J. Ito, *Laryngoscope* **2005**, *115*, 2016.
[4] K. Mizutari, M. Fujioka, M. Hosoya, N. Bramhall, H. J. Okano, H. Okano, A. S. B. Edge, *Neuron* **2013**, *78*, 403.
[5] M. Izumikawa, R. Minoda, K. Kawamoto, K. A. Abrashkin, D. L. Swiderski, D. F. Dolan, D. E. Brough, Y. Raphael, *Nat. Med.* **2005**, *11*, 271.
[6] K. Oshima, S. Suchert, N. H. Blevins, S. Heller, *J. Commun. Disord.* **2010**, *43*, 311.
[7] S. B. Waltzman, *Expert Rev. Med. Devices* **2006**, *3*, 647.
[8] M. K. Cosetti, S. B. Waltzman, *Expert Rev. Med. Devices* **2011**, *8*, 389.
[9] F. Y. Chen, H. I. Cohen, T. G. Bifano, J. Castle, J. Fortin, C. Kapusta, D. C. Mountain, A. Zosuls, A. E. Hubbard, *J. Acoust. Soc. Am.* **2006**, *119*, 394.
[10] H. Shintaku, T. Nakagawa, D. Kitagawa, H. Tanujaya, S. Kawano, J. Ito, *Sens. Actuators A* **2010**, *158*, 183.
[11] R. D. White, K. Grosh, *Proc. Natl. Acad. Sci. USA* **2005**, *102*, 1296.
[12] M. J. Wittbrodt, C. R. Steele, S. Puria, *Audiol. Neuro-Otol.* **2006**, *11*, 104.
[13] T. Xu, M. Bachman, F. G. Zeng, G. P. Li, *Sens. Actuators A* **2004**, *114*, 176.
[14] H. Shintaku, T. Kobayashi, K. Zusho, H. Kotera, S. Kawano, *J. Micromech. Microeng.* **2013**, *23*.
[15] T. Inaoka, H. Shintaku, T. Nakagawa, S. Kawano, H. Ogita, T. Sakamoto, S. Hamanishi, H. Wada, J. Ito, *Proc. Natl. Acad. Sci. USA* **2011**, *108*, 18390.
[16] E. Venkatragavaraj, B. Satish, P. R. Vinod, M. S. Vijaya, *J. Phys. D Appl. Phys.* **2001**, *34*, 487.
[17] K. I. Park, S. Xu, Y. Liu, G. T. Hwang, S. J. L. Kang, Z. L. Wang, K. J. Lee, *Nano Lett.* **2010**, *10*, 4939.
[18] X. D. Wang, J. H. Song, J. Liu, Z. L. Wang, *Science* **2007**, *316*, 102.
[19] M. Y. Choi, D. Choi, M. J. Jin, I. Kim, S. H. Kim, J. Y. Choi, S. Y. Lee, J. M. Kim, S. W. Kim, *Adv. Mater.* **2009**, *21*, 2185.
[20] X. Chen, S. Y. Xu, N. Yao, Y. Shi, *Nano Lett* **2010**, *10*, 2133.
[21] S. Xu, Y. Qin, C. Xu, Y. G. Wei, R. S. Yang, Z. L. Wang, *Nat. Nanotechnol.* **2010**, *5*, 366.
[22] G. A. Zhu, R. S. Yang, S. H. Wang, Z. L. Wang, *Nano Lett* **2010**, *10*, 3151.
[23] K.-I. Park, J. H. Son, G.-T. Hwang, C. K. Jeong, J. Ryu, M. Koo, I. Choi, S. H. Lee, M. Byun, Z. L. Wang, K. J. Lee, *Adv. Mater.* **2014**, *26*, 2514.
[24] G.-T. Hwang, H. Park, J.-H. Lee, S. Oh, K.-I. Park, M. Byun, H. Park, C. K. Jeong, K. No, H. Kwon, S.-G. Lee, B. Joung, K. J. Lee, *Adv. Mater.* **2014**, *26*, 4880.
[25] H. Davis, *Hearing Res.* **1983**, *9*, 79.
[26] B. N. Evans, P. Dallos, *Proc. Natl. Acad. Sci. USA* **1993**, *90*, 8347.
[27] J. Zheng, W. X. Shen, D. Z. Z. He, B. L. Kevin, L. D. Madison, P. Dallos, *Nature* **2000**, *405*, 149.
[28] M. C. Liberman, J. G. Gao, D. Z. Z. He, X. D. Wu, S. P. Jia, J. Zuo, *Nature* **2002**, *419*, 300.
[29] H. Shintaku, T. Inaoka, T. Nakagawa, S. Kawano, J. Ito, *J. Biomech. Sci. Eng.* **2013**, *8*, 198.
[30] G. V. Bekesy, *Nature* **1970**, *225*, 1207.
[31] C. R. Steele, L. A. Taber, *J. Acoust. Soc. Am.* **1979**, *65*, 1007.
[32] E. R. Camargo, J. Frantti, M. Kakihana, *J. Mater. Chem.* **2001**, *11*, 1875.
[33] X. Y. Zhang, X. Zhao, C. W. Lai, J. Wang, X. G. Tang, J. Y. Dai, *Appl. Phys. Lett.* **2004**, *85*, 4190.
[34] I. R. Henderson, *Piezoelectric Ceramics: Principles and Applications*, APC International, Mackeyville, PA **2002**.
[35] G. H. Haertling, *J. Am. Ceram. Soc.* **1999**, *82*, 797.
[36] M. A. Ruggero, N. C. Rich, *Hearing Res.* **1991**, *51*, 215.
[37] Y. Jung, J. H. Kwak, Y. H. Lee, W. D. Kim, S. Hur, *Sensors* **2014**, *14*, 117.
[38] A. N. Lukashkin, I. J. Russell, *J. Acoust. Soc. Am.* **2003**, *113*, 1544.